Airborne Measurement of Liquid and Total Water Content

GERMAN VIDAURRE* AND JOHN HALLETT

Desert Research Institute, Reno, Nevada

DAVID C. ROGERS

National Center for Atmospheric Research,+ Boulder, Colorado

(Manuscript received 4 November 2010, in final form 12 April 2011)

ABSTRACT

Two identical liquid water content (LWC) King probes—one total water content/liquid water content (TWC/LWC) Nevzorov probe and two constant-temperature T probes that are different in size to distinguish particles of different densities and diameters (section 2c)—were flown during the Alliance Icing Research Study (AIRS) II field campaign in the fall of 2003. This paper assesses measurements performed during several flights in mostly stratiform clouds. The two LWC King probes tracked well; however, discrepancies of up to 0.1 g m^{-3} for 1-s LWC measurements of 0.3 g m^{-3} were observed. Agreement between probes of different geometry and size was generally favorable, while levels of disagreement between the probes changed during numerous cloud penetrations from less than 20% up to a factor of 2, varying with flight conditions and microphysical structure of the cloud. Disagreement between probes was even larger when detecting ice water content (IWC). Measurement differences were attributed to different collection efficiencies resulting from preferred particle size, shape, and density and local aerodynamic effects around the aircraft. Measurements from a single probe are subject to uncertainty at a single point in time beyond the noise and drift level of the instrument. This uncertainty is evaluated considering particle habit, diameter, and density, and probe geometry and size, in addition to particle impact, breakup/splash, and bounce. From a working point of view, the intercomparison of several probes is subject to real but unknown spatial differences because of different locations between air samples. Comparison of identical probes is not appropriate because each measurement in itself is unique by definition. Thus, instead of duplication of instruments, subject to these levels of agreement, the use of a single probe is a practical approach while remaining aware of its limitations and capabilities.

1. Introduction

Mixed-phase conditions are relevant to cloud evolution, precipitation, radiation, and aircraft performance. A complete spatial characterization of the microphysical conditions leading to aircraft icing is necessary, along with a wider knowledge regarding the dataset extremes and the conditions under which they occur. Knowledge of the spatial distribution of liquid-only, ice-only, and mixed-phase regions is desirable in order to study both specific properties of the cloud and the design of instruments capable of detecting higher liquid water content (LWC) and the extremes of LWC.

Aircraft-mounted probes of different shapes and sizes, such as the King, T (see section 2c), and Nevzorov probes, are commonly used to characterize the cloud microphysical conditions leading to aircraft icing. Aircraft-mounted probes, limited by instrumental resolution, revealed narrow mixed-phase regions on the order of a few hundred meters and less (Vidaurre and Hallett 2009a). These probes have been individually tested and calibrated in the laboratory, and as part of a normal procedure they are referenced to clear-air conditions in each flight. However, the limitations and capabilities of each probe, because of their unique geometry and response to microphysical conditions, may be overlooked, compromising measurements and conclusions. When making

* Current affiliation: Texas A&M University, College Station, Texas.

+ The National Center for Atmospheric Research is sponsored by the National Science Foundation.

Corresponding author address: John Hallett, 2215 Raggio Parkway, Desert Research Institute, Reno, NV 89512.
E-mail: hallett@dri.edu

DOI: 10.1175/JTECH-D-10-05035.1

© 2011 American Meteorological Society

a physical measurement in the laboratory, under as identical physical conditions as possible, it is adequate to use a standard theory of error analysis to determine the uncertainty. This is an approach that is valid under controlled conditions (e.g., in a wind tunnel study), with application to instruments for aircraft measurement. On the other hand, an aircraft measurement in flight, as any measurement in the atmosphere, is itself unique. In this case, statistical evaluation provides application to a geophysical environment as the likelihood of meeting a given condition. Specific situations for test purposes provide useful comparisons, but not in the sense of a controlled experiment.

In addition, instruments mounted at different locations on an aircraft behave differently overall, apart from being located in known different environments. The aircraft also has a changing orientation (yaw and pitch) that can influence measurements; also, instruments on one or the other wingtip can be flown with one in and one out of a well-defined aircraft contrail. Assuming that flight is in a uniform environment is an erroneous course to steer. Analysis of data gathered with probes located at different places around the aircraft fuselage might provide useful insights about the microphysical structure of the cloud only if local aerodynamic effects and particle collection efficiency based on probe geometry and particle size, shape, and density are considered.

The Alliance Icing Research Study (AIRS) II (Bailey and Hallett 2009; Hudson 2007; Lasher-Trapp et al. 2008) was a project conducted in association with the Aircraft Icing Research Alliance (AIRA), which consists of organizations within North America interested in aircraft icing. The AIRS II campaign, building on the results of AIRS I, had the following objectives: (i) to develop techniques/systems to remotely sense hazardous winter conditions at airports, (ii) to improve weather forecasts of aircraft icing conditions, (iii) to collect data for flight validation methodologies, and (iv) to better characterize the aircraft-icing environment. Liquid water content measurements from two standard King probes mounted on identical locations on each side of the National Center for Atmospheric Research (NCAR) C-130 aircraft during the project are analyzed in order to study the effect of probe geometry and location. Simultaneous LWC measurements from these two probes and from the Nevzorov and small and large T probe measurements are evaluated. For completeness, ice water content (IWC) measurements from the latter three probes are also considered to study probe collection efficiency dependency on particle density. The bulk of the data was collected in stratiform clouds, in some cases associated with frontal systems and lake-effect convection.

2. Liquid water content and total/liquid water content probes

During the AIRS II project two LWC King probes were mounted on the NCAR C-130, one under each wing 3.2 m from the wingtip (Fig. 1). The two LWC King probes have flown in that location in several research projects. The wing span is 40.4 m, and the probes were separated by 34 m. The small total water content (TWC)/LWC T probe was mounted near the right wingtip; meanwhile the large TWC/LWC T probe was mounted on the fuselage about 14 m apart from one of the King probes, which is more convenient for the ½-kW power required (Fig. 1). The TWC/LWC Nevzorov probe was also mounted on the fuselage, about 1 m apart from the large T probe. Both probes were located about 0.5 m above the aircraft skin inside the region where particle sorting occurs (<0.61 m; see Twohy and Rogers 1993).

a. Liquid water content King probe

The LWC King probe (King et al. 1978) consists of a cylindrical sensor of 2-mm diameter that is orthogonal to the airflow. It requires at most a dry calibration; it has a sensitivity of 0.02 g m^{-3}, has a response time (the time required for a signal to go from 10% to 90% of a step change) of the order of 0.05 s, and has a precision of about 5% at 1 g m^{-3}. King probe measurements may also be influenced by particle shattering on the surface of the housing parts ahead of the sensor and by direct impact. The significance of this breakup effect is still to be determined. The relative impact kinetic energy to surface energy ratio (E_K/E_σ), given by a modified Weber number L, characterizes the breakup process (Hallett and Christensen 1984; Vidaurre and Hallett 2009b). For convenience, E_σ is defined as the surface energy of a spherical particle; thus, L is given by

$$L = \frac{E_K}{E_\sigma} = \frac{\frac{1}{2}\left(\frac{\pi}{6}D^3\rho\right)U^2}{\pi D^2\sigma} = \frac{D\rho U^2}{12\sigma},$$

where D is the particle diameter, ρ the density, σ the water surface energy, and U the impact velocity. It measures the amount of deformation of the particle and the maximum possible surface area increase at impact.

Drops splash when impacting on rough surfaces for $L > 7$ and smooth surfaces for $L > 20$ ($\sigma_w = 0.073$ J m^{-2} at 20°C), with more energy being required for splashing to occur on smooth surfaces than rough surfaces.[1] The

[1] For a very smooth surface the initial incoming energy is converted into radial flow on the surface and a spreading of the drop occurs on an expanding and thinning disk before any breakup.

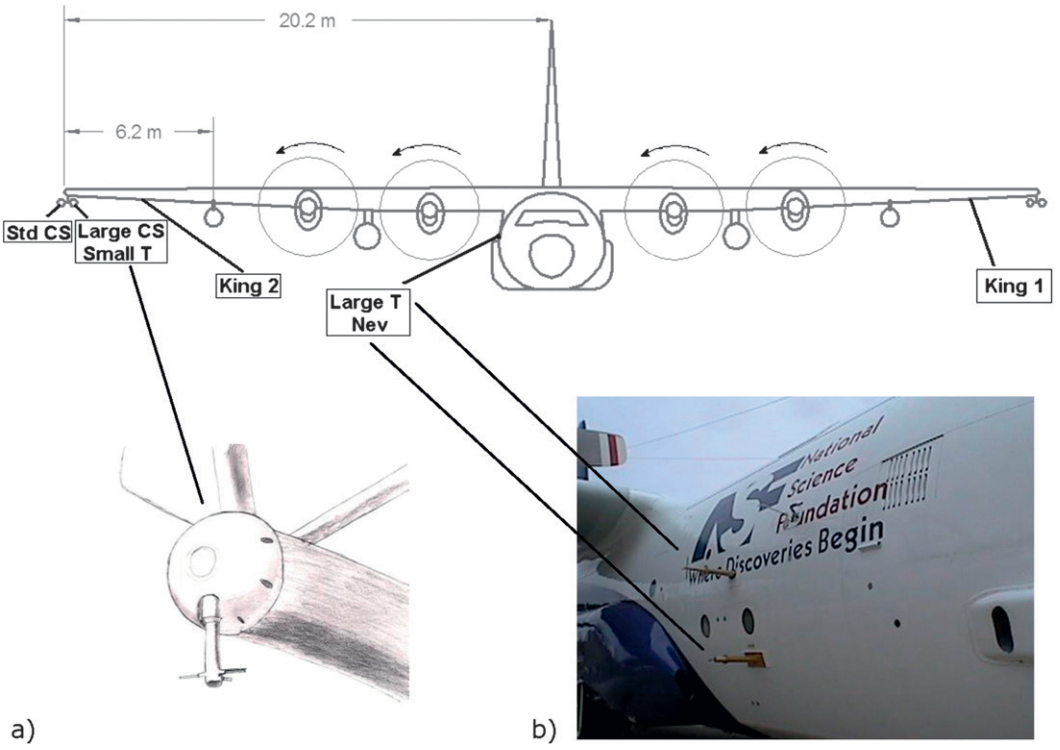

FIG. 1. Probe location on NCAR C-130 during the Alliance Icing Research Study II. (from left to right) (a) The standard cloud scope, the large cloud scope coupled with the small T probe, and the second King probe mounted in the right wing; and (b) the large T probe and Nevzorov probe on the fuselage. The first King probe was mounted on the left wing.

process of ice breakup ($\sigma_i = 0.120$ J m^{-2} at 20°C) is more complex and the value of L applicable to ice breakup depends on the physical detail of the impaction.

Figure 2 (top left) shows the kinetic-to-surface energy ratio L for spherical droplets impacting a 2-mm-diameter cylinder (solid), such as the King probe sensor and a 2-cm-diameter cylinder (dashed) similar in size to the housing of the King probe located upstream of the sensor. On approach, particles decelerate from an original speed relative to the cylinder of 130 m s^{-1} to a lower impact velocity (estimated from trajectory calculations); they may also never impact at all. Here, $L = 7$ provides the water droplet breakup criterion. Particles of a diameter smaller than 50 μm impacting with $L > 7$ are subject to splash, while larger particles impacting with $L \gg 7$ are subject to severe splash (many small particles generated). For comparison, Fig. 2 also shows the kinetic-to-surface energy ratio L for spherical ice particles of different densities (920, 460, and 230 kg m^{-3}). The occurrence of breakup and its severity depends on particle size and density, making larger particles and/or denser ones more susceptible to breakup. The distribution of the kinetic energy during impact is still to be determined, along with the influence of the generated particles on the King probe measurements resulting from either particle loss (by bounce) or the capture of droplets generated on impact upstream of the sensor.

b. Nevzorov probe

The Nevzorov LWC/TWC probe (Isaac et al. 2006; Korolev and Strapp 2002; Korolev et al. 1998) consists of two different sensors for measurement of TWC and LWC, the difference of which yields IWC. The LWC sensor has a half-cylinder shape with 1.5-mm diameter. The TWC sensor is an 8-mm-diameter concave cone, which faces the flow and works as a trap for impacting cloud particles. The Nevzorov probe swivels to align with airflow. Its alignment capability may be a source of error due to an adjusting lag between the probe alignment and continuous changes in the aircraft attack angle. The alignment time could be estimated from the probe response during porpoise maneuvers involving rapid changes in the angle of attack.

c. T probe

The T probe assembly consists of three separate sensors arranged as a T (Fig. 3a): a cylindrical sensor axis transverse to the airflow, which collects most of the

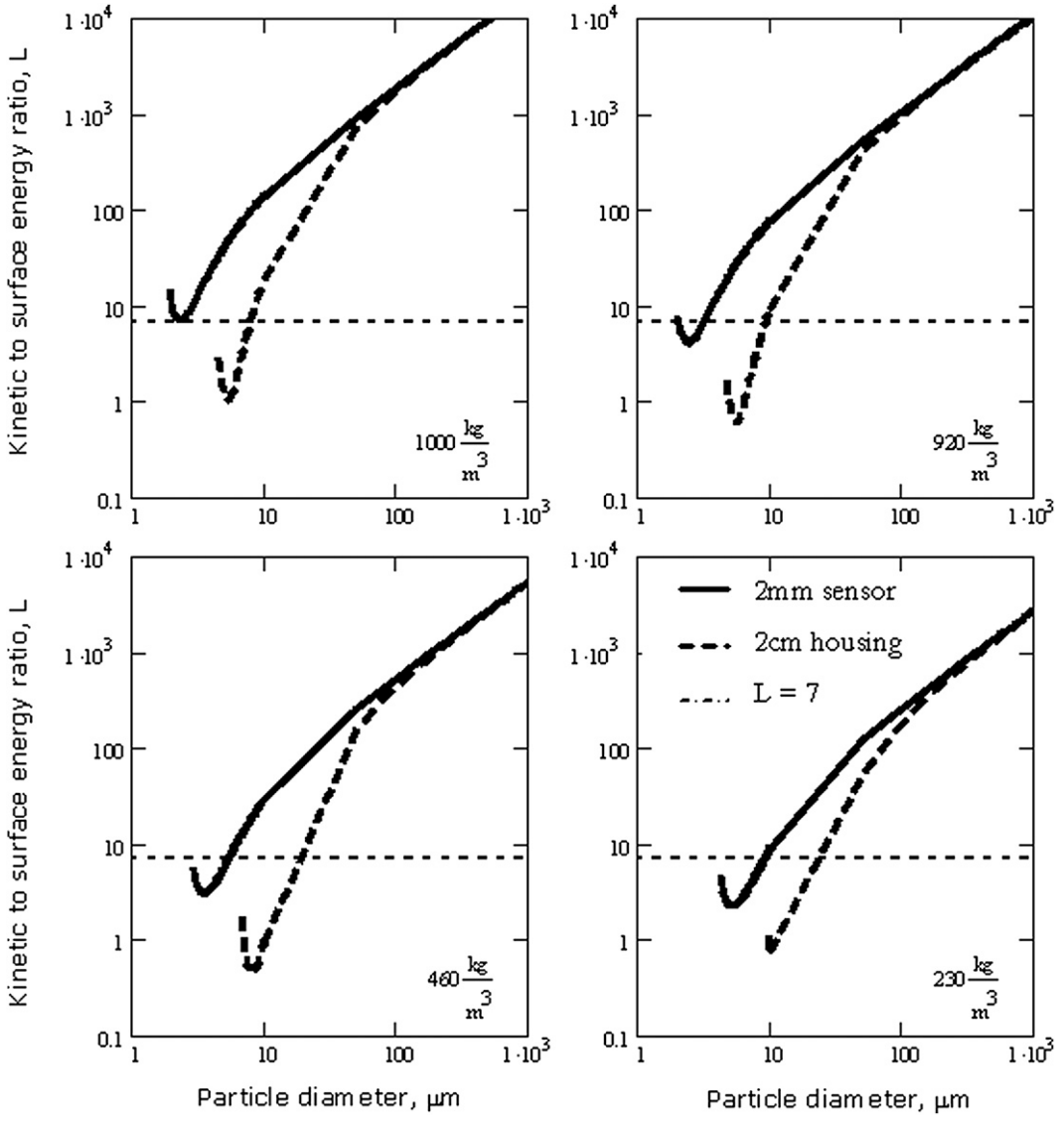

FIG. 2. (top left) Kinetic-to-surface energy ratio for spherical droplets and spherical ice particles of different density impacting a 2-mm-diameter cylinder (solid), such as the King probe sensor, and a 2-cm-diameter cylinder (dashed) similar in size to the housing of the King probe, located upstream of the sensor.

impacting water (Fig. 3b); a cylinder with a V-shaped cut along its axis, also transverse to the airflow, which collects most of the impacting water and ice particles (Fig. 3c); and a backward-facing cylindrical reference sensor, identical in shape to the first sensor, which ideally collects neither ice nor water and is subject only to heat transfer to the airflow (Hallett et al. 2005; Vidaurre and Hallett 2009a). The T probe operates by measuring the electrical power required to maintain near-constant temperature during accretion and evaporation of water and/or ice, together with cooling resulting from ambient flow of air at differing pressures, temperatures, and hence densities. Thus, the sensors have a function similar to the hot-wire probe for measurement of liquid water (King et al. 1978), the ice sensor (Hallett 1980; King and Turvey 1986), and the Nevzorov probe (Korolev et al. 1998).

Figure 3 shows both small and large T probes. The small T probe of a projected area of 4 mm $\times$ 40 mm collects small particles and low-density particles that might not be collected by the large T probe of a projected area of 10 mm $\times$ 70 mm. The instruments are designed to be sufficiently robust to survive aircraft icing conditions and particle impact at flight speed through clouds and precipitation. The small T probe has flown mounted on the NCAR C-130 and Convair 580 at speeds of about 150 m s^{-1} without any problem. The shape of the total

FIG. 3. T probes showing (a) assembly of large and small T probes; (b) 1-cm-diameter by 7-cm-long large T probe sensor, with an axis transverse to the airflow to collect most of the impacting water; and (c) large T probe reentrant cylinder also transverse to the airflow, with a 1 cm × 7 cm projected area, to collect most of the impacting water and ice. (b) and (c) A backward-facing cylindrical reference sensor, also shown, is similar to the one used to collect impacting water, collecting little ice or water and being subject only to the airflow and conditions of the ambient air.

sensor improves collection by recapturing ejected particles and fragments produced during direct impact with the sensor, as observed during wind tunnel experiments at low airspeed (40 m s^{-1}; see Vidaurre and Hallett 2009b). A fraction of these particles bounced off along the axis of the sensor to eventually impact the sensor surface again; meanwhile, other fragments bounced off in an orientation across the sensor into the airstream. These experiments suggested that the large surface area of the T probe total water sensor reduces the losses resulting from bouncing. Additionally, the T probes allow the adjustment of the operational temperature of the probe; increasing it enhances evaporation by reducing the fraction of particles that bounce off. Quantitative experiments are still necessary for an adequate evaluation of the effect on measurements conducted with the T probe and other probes, such as the Nevzorov probe.

Water content is inferred from the differential power between the water sensor and the reference sensor. A second-order correction may be applied for ice collected on the water probe at the forward-edge stagnation line. An estimate of any false indication by ice at the stagnation line of the water sensor is obtained by calibration during flight in a known all-ice cloud ($T < -40$°C) to be below 0.02 g m^{-3}, and in some cases as low as 0.005 g m^{-3}, as shown in Fig. 4. This uncertainty is equivalent to a pseudoadiabatic rise of 10 mb. Ice content is computed from the total sensor power that is differenced by water sensor power. Raw power measurements are corrected for airspeed, temperature, and density, and then are related through the latent heat of evaporation to the mass accretion rate of each sensor, and ultimately lead to integrated particle mass through the penetrated volume. The thermal response time of the two T probes is of the order of 0.1 and 1 s, corresponding to a flight path of some 10 and 100 m for an aircraft speed of 100 m s^{-1}. The sensor temperature is adjustable in software for likely values of ice water content and penetration velocity over the range from 100° to currently 165°C for prompt evaporation prior to bounce-off of TWC to a maximum of 1 g m^{-3}, without affecting heat transfer or melting the solder.

Power requirements in clear air are not the same for the liquid water, total water, and reference sensors of the T probe because of differences in shape and location. Subtracting the difference between the power required by each sensor in clear air adjusts the instrument's "zero value." Because the total sensor does not have a simple shape, there is no background of empirical data describing the factors affecting the heat transfer. However, the power demanded by each sensor of the T probe can be estimated from measurements of temperature, pressure, airspeed, and aircraft attack angle. The selection of these variables is the result of a correlation analysis performed on part of the AIRS II data. This approach differs from the calibration method of the King probe suggested in King and Turvey (1986) and King et al. (1978). The difference between the total and water sensors and between the water and reference sensors during clear-air events is fitted by an empirical second-degree multipolynomial relationship as follows:

$$Pd_1 - Pd_2 = \sum_i^n \mathbf{b}_i p^{\mathbf{x}_{i,0}} T_e^{\mathbf{x}_{i,1}} v^{\mathbf{x}_{i,2}} \alpha^{\mathbf{x}_{i,3}},$$

where **b** is the coefficient vector, **x** the exponent matrix, v the true airspeed, p the pressure, T_e the ambient temperature, and α the aircraft attack angle. Figure 5 shows required power by LWC and IWC and their estimates during clear air.

STATISTICAL ANALYSIS OF THE NOISE AND DRIFT ASSOCIATED WITH T PROBE MEASUREMENTS

Quantifying the uncertainty of the T probes is a complex problem to be answered empirically. There are

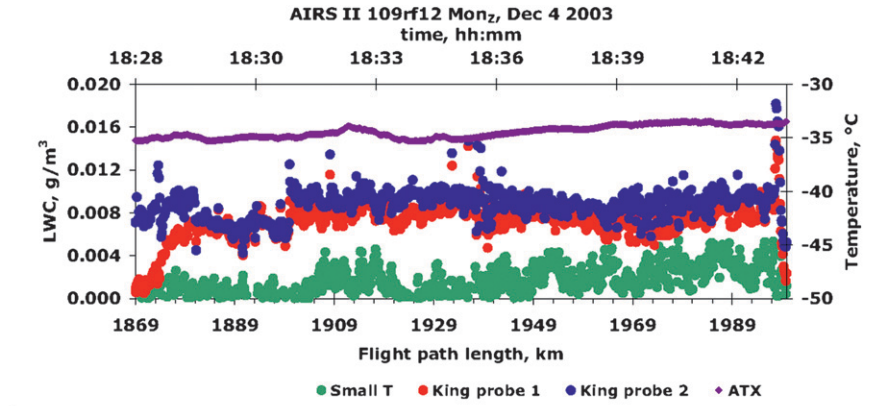

a)

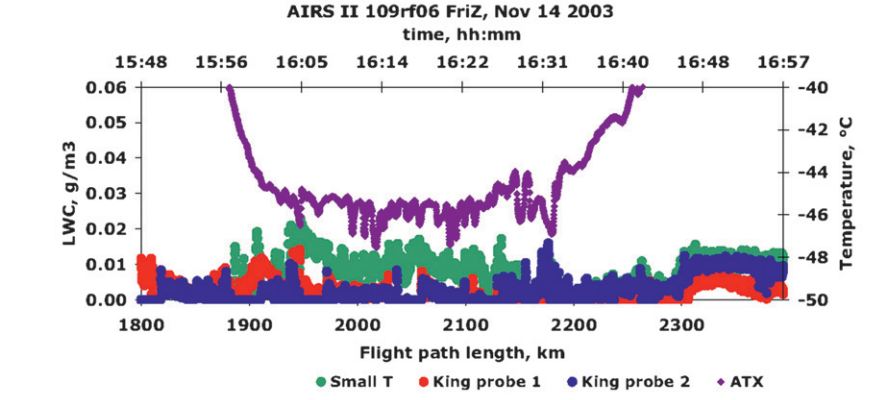

b)

FIG. 4. Sensitivity of water sensor to ice accretion: T probe and King probe LWC measurements during flight in known all ice cloud (ambient air temperature ATX < -38°C) events in (a) 4 Dec 2003 and (b) 14 Nov 2003 provide an estimate of the upper limit of the false indication by ice collected at the stagnation line of the water sensor.

several sources of uncertainty in the calibration and algorithm technique used, which will affect the final output.

Clear-air data were used to run a specific calibration for each flight. True airspeed, air temperature, corrected air pressure, and attack angle were the independent variables used. The output data provided an idea of the noise and drift of the ice and liquid water content measurements. In case no true airspeed data are available or local aerodynamic effects around the probe location may have induced a different local airspeed at the probe location, the calibration could be set up to estimate the airspeed based on air temperature, pressure, attack angle, and reference sensor power requirement. Tables 1 and 2 show the mean value and standard deviation of the clear-air data used for each flight during the AIRS II campaign. In general, all flights present a zero mean value and standard deviation below 0.02 g m^{-3}. The 97.5 percentile of clear-air data (the value below which 97.5% of the clear-sky data fell), also shown, provided better estimates of the uncertainty associated with the IWC and LWC measurements. It was below 0.02 g m^{-3} for most AIRS II flights, and below 0.01 g m^{-3} in some cases. It is a factor 1.75 smaller than similar measurements of the Nevzorov airborne hot-wire LWC/TWC probe, and at least a factor of 8 less than similar measurements of the King liquid water probe on the Canada Environment Convair 580 aircraft (Korolev and Strapp 2002).

3. Probe particle collection efficiency

Figure 6 shows King, LWC Nevzorov, small and large T probes (cylindrical sensors), and conical TWC Nevzorov collection efficiencies of particles of different sizes and densities at -16°C, 700 mb, and 115 m s^{-1}. The collection efficiency of the Nevzorov LWC/TWC probe is reported in Korolev et al. (1998); meanwhile,

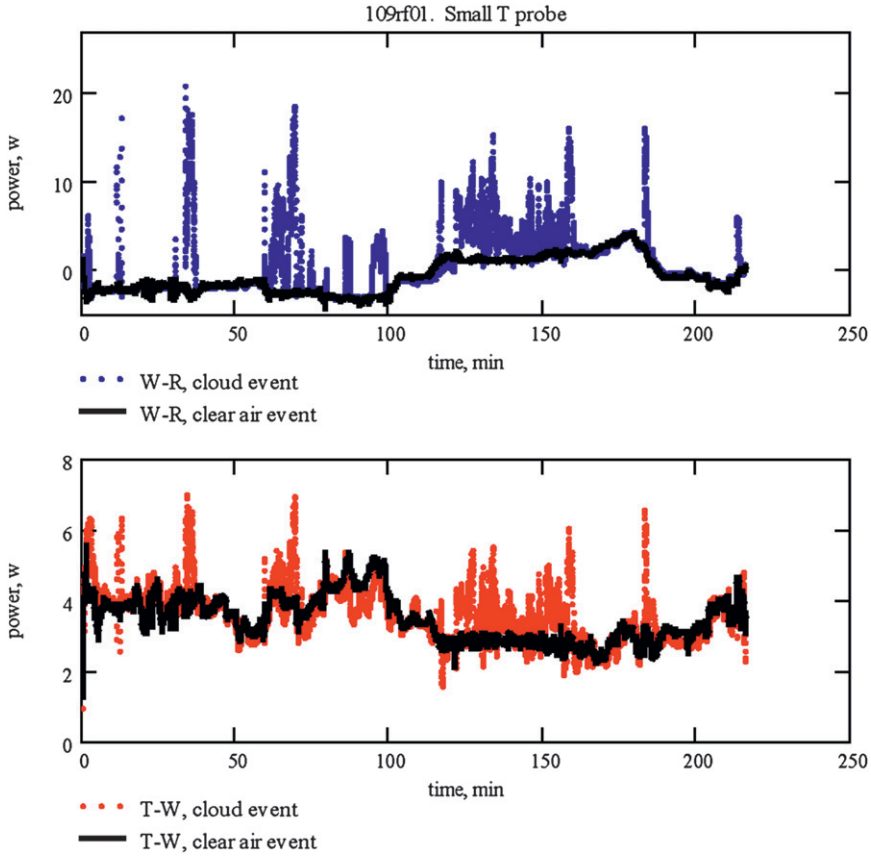

FIG. 5. Small T probe power demanded by liquid-only (blue), ice-only (red), and dry heat transfer (black) during the AIRS II flight 109rf01 on 5 Nov 2003. The power required to evaporate liquid only is estimated as the difference between the power consumed by the cylindrical sensor (W) to the reference sensor (R). The power required to evaporate ice only is estimated as the difference between the power consumed by the total sensor (T) to the cylindrical sensor (W).

the collection efficiency of the other probes, defined as the fraction of small spherical particles in air moving at high velocity v that impacts with a cylinder of radius C in their trajectory, is estimated following Langmuir and Blodgett (1946) and Ranz and Wong (1952). In the case of droplets of 10-μm diameter and 1000 kg m^{-3} density, about 0.9 of them get captured by the LWC Nevzorov probe and 0.6 by the TWC Nevzorov probe; these two values are the highest and lowest collection efficiencies among the considered probes. The collection of same-sized particles but with densities of 100 kg m^{-3} is now 0.6 for the small T probe and 0.1 for the large T probe. This fact suggests that the collection capability of the instruments is highly sensitive to the density of the particle, a property that is quite often overlooked. In this manner, a comparison of the measurements of dynamically similar but different dimension probes leads to improved characterization of the particle density.

a. Particle density

Estimation of the probe collection capability requires knowing particle density. Bulk water density (1000 kg m^{-3}) is used when considering droplets; meanwhile, the density of ice particles can range from 20 to 920 kg m^{-3} (Hallett and Garner 2010). The following sections present three different methods that are used to estimate the density of ice crystals.

1) USE OF DATA FROM SEVERAL PROBES

By the use of a bootstrapping subroutine (Davison and Hinkley 1997), the density of spherical particles (ρ_s) of radius a is estimated using the following equation:

$$\rho_s = \frac{\mathrm{IWC}}{N\frac{4\pi}{3}a^3},$$

where, in addition to variables previously described, N is the particle number concentration. The forward scattering

TABLE 1. IWC and LWC large T probe average, standard deviation, and 97.5 percentile clear-air data used to estimate the measurement uncertainty for each flight during AIRS II.

	IWC (g m^{-3})			LWC (g m^{-3})		
Flight No.	Mean	Std dev	97.5%	Mean	Std dev	97.5%
109rf01	0.000	0.005	0.008	0.000	0.004	0.009
109rf02	0.000	0.010	0.016	0.000	0.008	0.014
109rf03	0.000	0.010	0.016	0.000	0.007	0.013
109rf04	0.000	0.009	0.016	0.000	0.006	0.011
109rf05	0.000	0.009	0.020	0.000	0.010	0.017
109rf06	0.000	0.010	0.019	0.000	0.009	0.016
109rf07	0.000	0.005	0.009	0.000	0.005	0.009
109rf08	0.000	0.006	0.011	0.000	0.006	0.011
109rf09	0.000	0.012	0.026	0.000	0.010	0.019
109rf10	0.000	0.009	0.016	0.000	0.007	0.012
109rf11	0.000	0.005	0.008	0.000	0.004	0.008
109rf12	0.000	0.007	0.014	0.000	0.009	0.020
109rf13	0.000	0.010	0.017	0.000	0.009	0.017
109rf14	0.000	0.007	0.014	0.000	0.007	0.015

TABLE 2. IWC and LWC small T probe average, standard deviation, and 97.5 percentile clear-air data used to estimate the measurement uncertainty for each flight during AIRS II.

	IWC (g m^{-3})			LWC (g m^{-3})		
Flight No.	Mean	Std dev	97.5%	Mean	Std dev	97.5%
109rf01	0.000	0.019	0.017	0.000	0.023	0.038
109rf02	0.000	0.013	0.014	0.000	0.010	0.014
109rf03	0.000	0.006	0.011	0.000	0.004	0.008
109rf04	0.000	0.004	0.010	0.000	0.003	0.005
109rf05	−0.001	0.010	0.021	−0.002	0.011	0.010
109rf06	0.000	0.008	0.018	0.000	0.011	0.015
109rf07	0.000	0.003	0.007	0.000	0.003	0.005
109rf08	0.000	0.006	0.013	0.000	0.005	0.007
109rf09	0.000	0.009	0.023	0.000	0.008	0.018
109rf10	0.000	0.008	0.020	0.000	0.005	0.007
109rf11	0.000	0.004	0.009	0.000	0.002	0.005
109rf12	0.000	0.008	0.015	0.000	0.006	0.014
109rf13	0.000	0.005	0.011	0.000	0.009	0.016
109rf14	0.000	0.007	0.014	0.000	0.005	0.009

spectrometer probe (FSSP), 2D cloud (2D-C) probe, and 2D precipitation (2D-P) probe provide N and particle diameter for different particle size ranges; meanwhile, T, Nevzorov, and counterflow virtual impactor (CVI) probes provide IWC. All measurements must be corrected depending on individual instrument collection capability. However, Gardiner and Hallett (1985) suggested that the FSSP gives a false response in ice clouds and it should not be used for characterization of small ice particles. Emery et al. (2004) observed the impact of ice particles with the hot-wire sensing element of the Nevzorov TWC/LWC probe, Science Engineering Associates TWC probe, and King LWC probe; in some cases the ice particles shattered into multiple smaller fragments, some of which rebounded off the sensor surface into the airstream and were swept away. Korolev et al. (2011), Vidaurre and Hallett (2009b), and references therein provide more details on particle breakup and its effect on aircraft probe measurements.

2) USE OF SURFACE AREA RATE DURING SUBLIMATION

The second method (Hallett et al. 1998) uses images of ice particles sublimating after impact with a surface to provide a local estimation of the ice particle density. The inverse of the rate of change of the surface area of a collapsed particle is related with its density, assuming it is constant over time and not a function of the radius, as follows:

$$\rho = \frac{2\pi K(T_E - T_s)}{L_{\text{sub}}(T_s)} \frac{1}{\dfrac{dA}{dt}},$$

where K is the air thermal conductivity; T_E and T_s the ambient and particle temperature at the surface, respectively; L_{sub} the water latent heat of sublimation at T_s; and dA/dt the rate at which the surface area of the collapsed particle decreases.

3) USE OF MASS–DIMENSION RELATIONSHIPS

Mass–dimension relationships were derived from particle size distributions measured with the Particle Measuring System FSSP monoprobe (5–56 μm), 2D-C imaging probe (from 33 to above 1000 μm), and 2D-P (200–6000 μm) imaging probe. They were used to compute the total particle volume per unit volume of air, assuming that the particles were spheres. Simultaneous measurements of ice water content were done with a CVI, yielding estimations of the overall effective ice density (Heymsfield et al. 2004). Because of the considerable amount of natural variability, no single relationship can be applied to all situations.

As mentioned above, the PMS probes and the CVI are subject to particle breakup. The CVI does prevent low-inertia particles ($D < 8$ μm) from entering the counterflow, while high-inertia particles follow the sample flow to whatever instrumentation is downstream of the CVI (Noone et al. 1988; Twohy et al. 1997; Twohy et al. 2003). Although fragments generated due to upstream impact are prevented from interfering with the sensing element, large particles may still impact internal surfaces and breakup because of airflow stress. Indeed, breakup of drops $D > 5$ μm was observed to influence CVI performance on tests at velocities above 153 m s^{-1} (Schwarzenbock and Heintzenberg 2000), yielding $L > 133$ (Vidaurre and Hallett 2009b). The effect

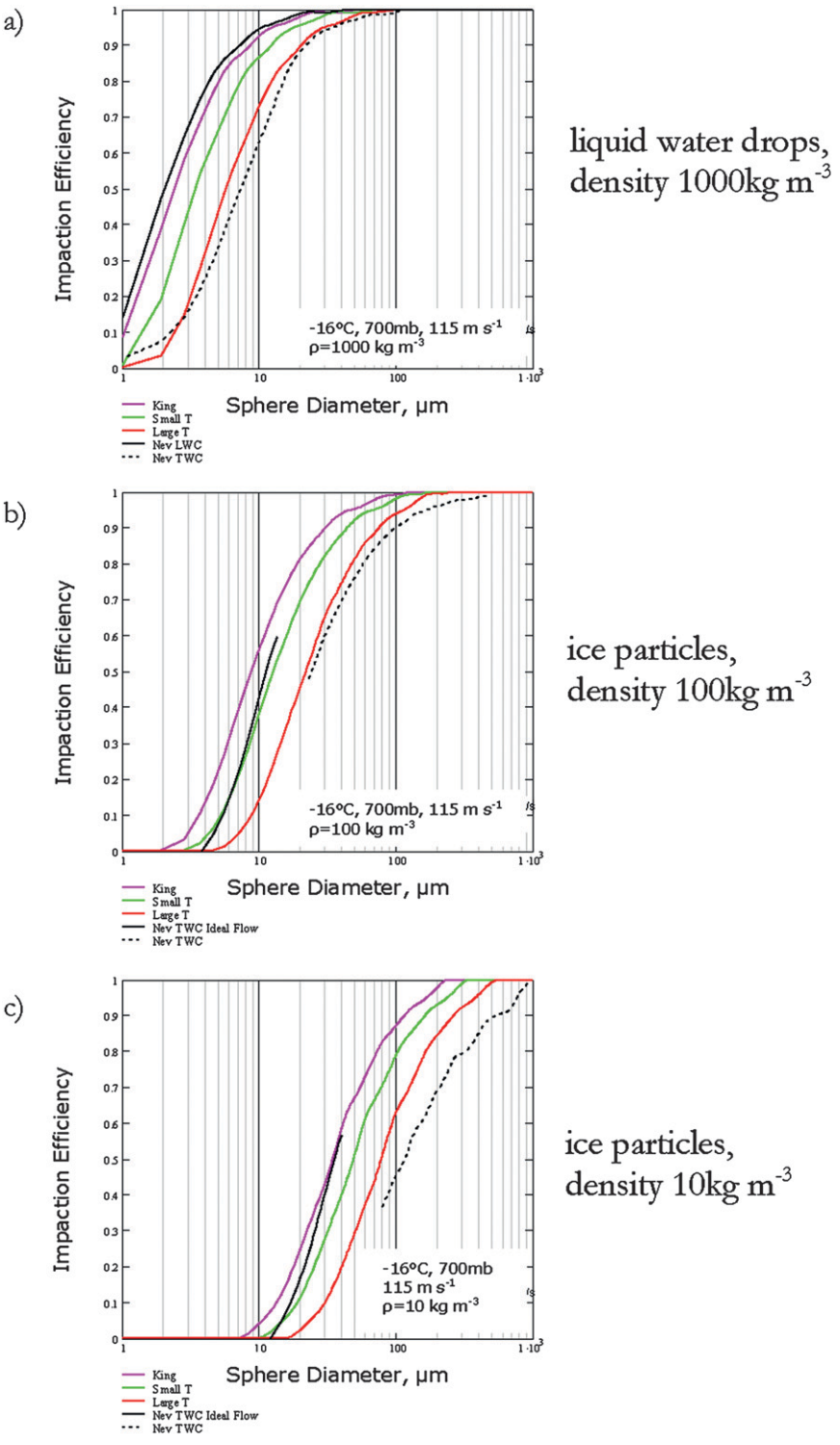

FIG. 6. Cylindrical King probe (2-mm diameter), LWC Nevzorov sensor (1.5 mm), small T probe (4 mm), large T probe (10 mm), and conical TWC Nevzorov sensor (8 mm) collection efficiency of spherical particles of (a) 1000 kg m^{-3}, (b) 100 kg m^{-3}, and (c) 10 kg m^{-3} density moving at 115 m s^{-1}, 700 mb, and −16°C. The collection efficiency of the probe is estimated as the fraction of spherical particles in air moving at high velocity that impacts with a cylinder in their trajectory (Langmuir and Blodgett 1946; Ranz and Wong 1952). In the case of the conical TWC Nevzorov sensor, the collection efficiency of particles 1000 kg m^{-3} in density is reported in Korolev et al. (1998) and for low density particles it is estimated from Langmuir and Blodgett (1946).

of particle breakup on the effective ice particle densities derived by this method is still to be determined.

4. King, Nevzorov, and T probes measurement data

Comparison between probes is a complex problem because probes of different sizes and shapes have different collection efficiencies and discrimination capabilities. For an optimal comparison, probes should be mounted on the aircraft as close as possible to each other so they sample a small region that represents the same air parcel. If they are located in different places around the aircraft fuselage, which is the case during the AIRS II project because of practical limitations and actual needs of each probe, then local airflow may influence probe performance in different ways.

a. Measurements from two standard King probes

Figure 7 shows a 22-min segment that is chosen to illustrate a variety of measurements from the AIRS II 109rf07 flight on 17 November 2003. This time period was a mostly straight and level leg (descending from 2000 to 1850 m MSL) in supercooled stratocumulus clouds. The aircraft's true airspeed was 112 m s^{-1} during this interval. Analog voltages from the King probes were sampled at 10 kHz and filtered down to 25 Hz (high-rate data) and 1 Hz (low-rate data). Inter Range Instrumentation Group (IRIG)-B time signals are sent to each data acquisition node to ensure the synchronization of all analog signals to within a few microseconds. The probes tracked closely together, reflecting the cloud structure (top panel), and yet there are significant differences at about 1-s intervals, as shown in the middle and lower panel. The difference between measurements, up to ± 0.1 g m^{-3} in some cases, and correlation between probes are plotted. These measurements are highly correlated ($r = 0.97$) at 25 Hz. The power spectra show no roll-off and no evidence of a noise floor or drift out to 12.5 Hz. The phase and cospectra plots suggest that these data are coherent to ~5 Hz. In general, the agreement between the two King probes is very good, especially when considering the large time periods in the comparison. When considering short time periods, the large discrepancies between the two King probes might be of importance because they can be attributed to spatial variations of the cloud in high gradient areas, meanwhile small differences in the scatter diagram can probably be attributed to the probe calibrations (power gain of the King probe output or errors in the sample areas) and noise.

b. Comparison between King, Nevzorov, and T probes

1) LWC MEASUREMENTS

Figure 8 shows the same selected high-rate measurements from the NCAR C-130 aircraft as depicted in Fig. 7, where the two King probe measurements are now plotted along with Nevzorov and small and large T probe measurements.[2] Each probe has a different shape and/or size; therefore, measurements must be corrected based on collection efficiency and local aerodynamic effects around the fuselage for a proper comparison. These corrections were not applied in Fig. 8 in order to compare the datasets as they are released after quality control.

The top panel in Fig. 8 shows a strong correlation (>0.92) between the small and large T, Nevzorov, and King probes. In general, all of the probes responded at the same time to changes in liquid water content, and differences in measurements were below the uncertainty of the instruments for probes of similar sizes and below a factor of 2 when compared to a large sensor (large T probe) with a small sensor (LWC Nevzorov). Some of this difference is due to the effects of local aerodynamic effects around the aircraft fuselage and actual variations in the cloud LWC, and some of the difference is due to the collection efficiencies. The last part, often ignored, can be easily estimated when information regarding particle density and size is available. Particle collection efficiencies of all of the probes considered in this paper were estimated when analyzing the AIRS II data as the necessary information was available.

The droplet concentration, given in the third panel, was about 400 cm^{-3}. The FSSP reported primarily small particles of 8-μm diameter (fourth panel). Only in a small region around 1835 UTC larger particles were detected by the 2D-C probe. Ambient temperature (ATX), plotted in the second panel, was −2°C, and the total air temperature (TTX), resulting from ram heating, was +5°C; hence the Rosemount icing probe (RICE) did not show ice accumulation (right side of top panel; TTX > 0°C).

Figure 9 shows LWC measurements during different periods of the AIRS II 109rf01 flight on 5 November 2003. Supercooled liquid conditions prevailed during most of the flight and no ice particles were detected. Ice accretion on the wings of the aircraft was observed in a few occasions during the flight. The top plot in each figure shows measurements from all of the indicated

[2] Nevzorov and King probe data were provided by NCAR on 8 September 2004 after the corresponding quality control. Small and large T probe data were provided by the Desert Research Institute (DRI) around the same time and in a similar way, after the corresponding quality control.

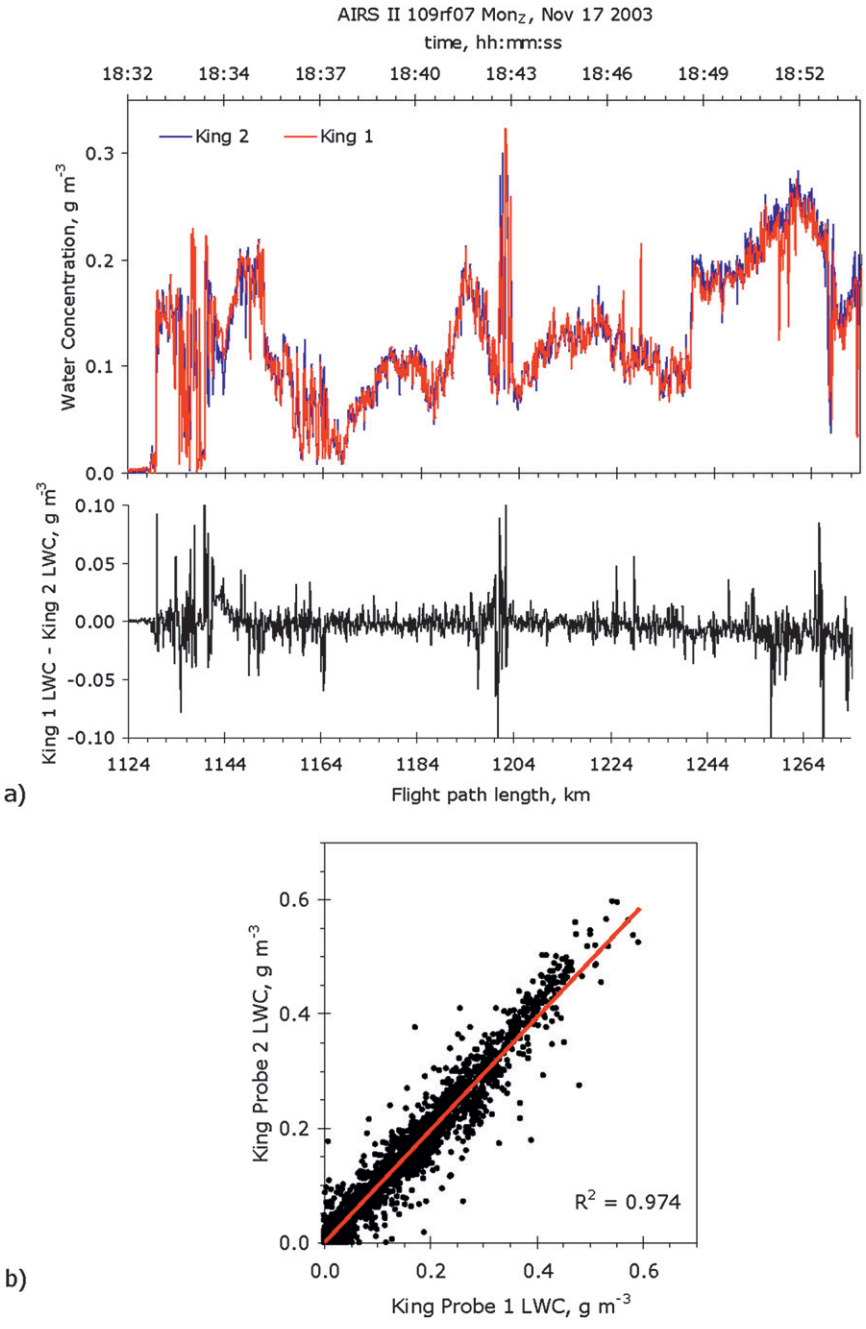

FIG. 7. (a) (top) LWC measurements from two King hot-wire probes during flight AIRS II 109rf07 on 17 Nov 2003 and (bottom) the difference between measurements in the lower panel. (b) 45° plot of LWC measurements from both King probes showing the correlation between them. The probes were mounted on the NCAR C-130 aircraft, one under each wing 3.2 m from the wingtip. The wing span is 40.4 m, and the probes were separated by 34 m.

probes. The lower plot shows only measurements from the two King probes. In general, inconsistencies in the relative response of the instruments are significant. They can be attributed to differences in probe shape and size, location around the aircraft, and probe response to cloud variations in composition and microphysical conditions. In Fig. 9a all of the probes agreed quite well with differences in the order of 10%–20%. King probe 2 (LWC2_Kin) and Nevzorov measured higher LWC than the other probes during the first part of the segment;

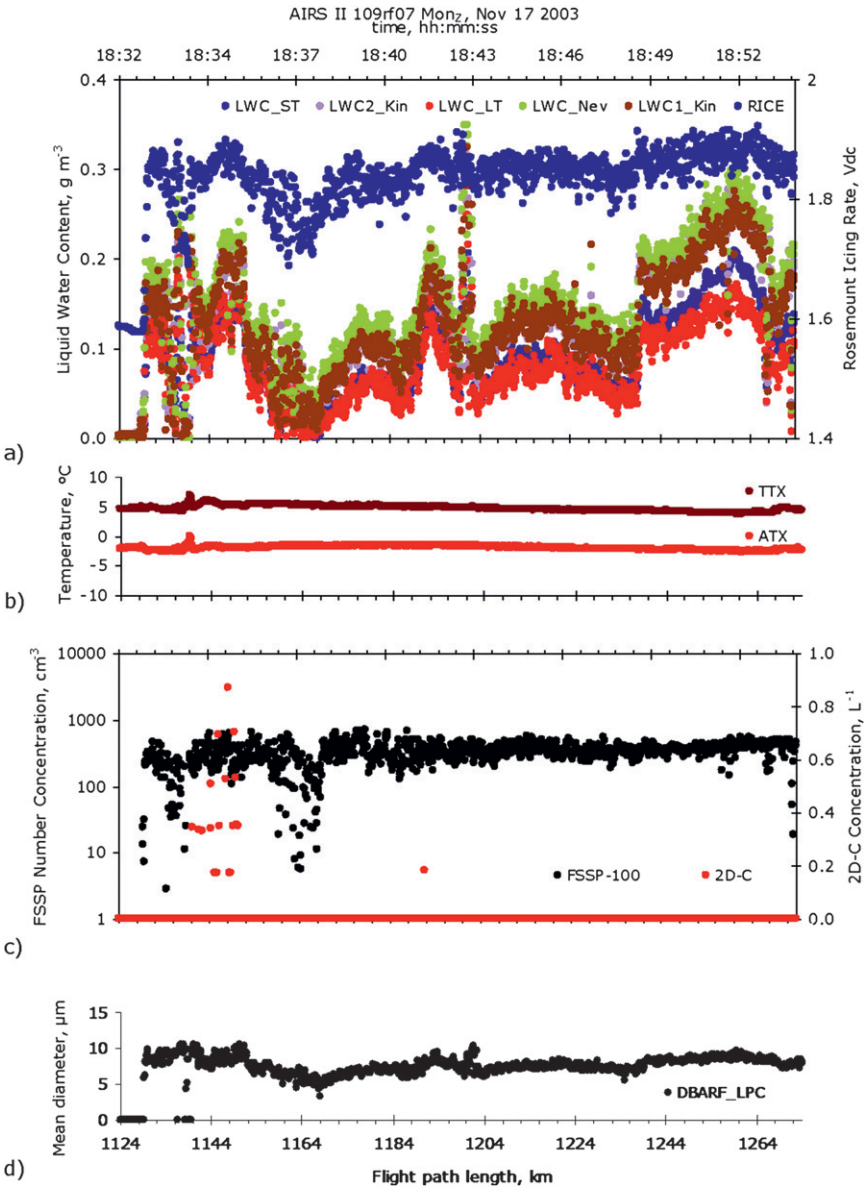

FIG. 8. (a) Liquid water content measurements from two King probes (LWC1_Kin and LWC2_Kin), small and large T probes (LWC_ST and LWC_LT), and Nevzorov (LWC_Nev) probes along with Rosemount icing rate (RICE) during AIRS II 17 Nov 2003. (b) ATX and TTX at the instrument surface. (c) Particle number concentration and (d) size measurements collected using the FSSP and 2D-C probes.

meanwhile, the other King probe agreed with the small T probe for most of the interval. The lower plot shows a strong disagreement between the two King probes up to 20% in some cases. This disagreement is even larger in Fig. 9b, where King probe measurements differed by a factor of 2. The responses of the two King probes in Figs. 9a,b are consistent with the observations plotted in Fig. 7. In Fig. 9a, the small T probe (red) agrees with one of the King probes (solid black), while the Nevzorov probe (green) agrees with the other King probe (dashed black). In Fig. 9b, the agreement between the two King probes and the Nevzorov probe is remarkably good, while the two T probes indicate lower LWC.

In contrast with Figs. 9a,b, Fig. 9c shows remarkably good agreement between the two King probes and Nevzorov probe. The difference between the two King probes can be explained by a baseline offset. The large T probe reported a slightly lower particle number

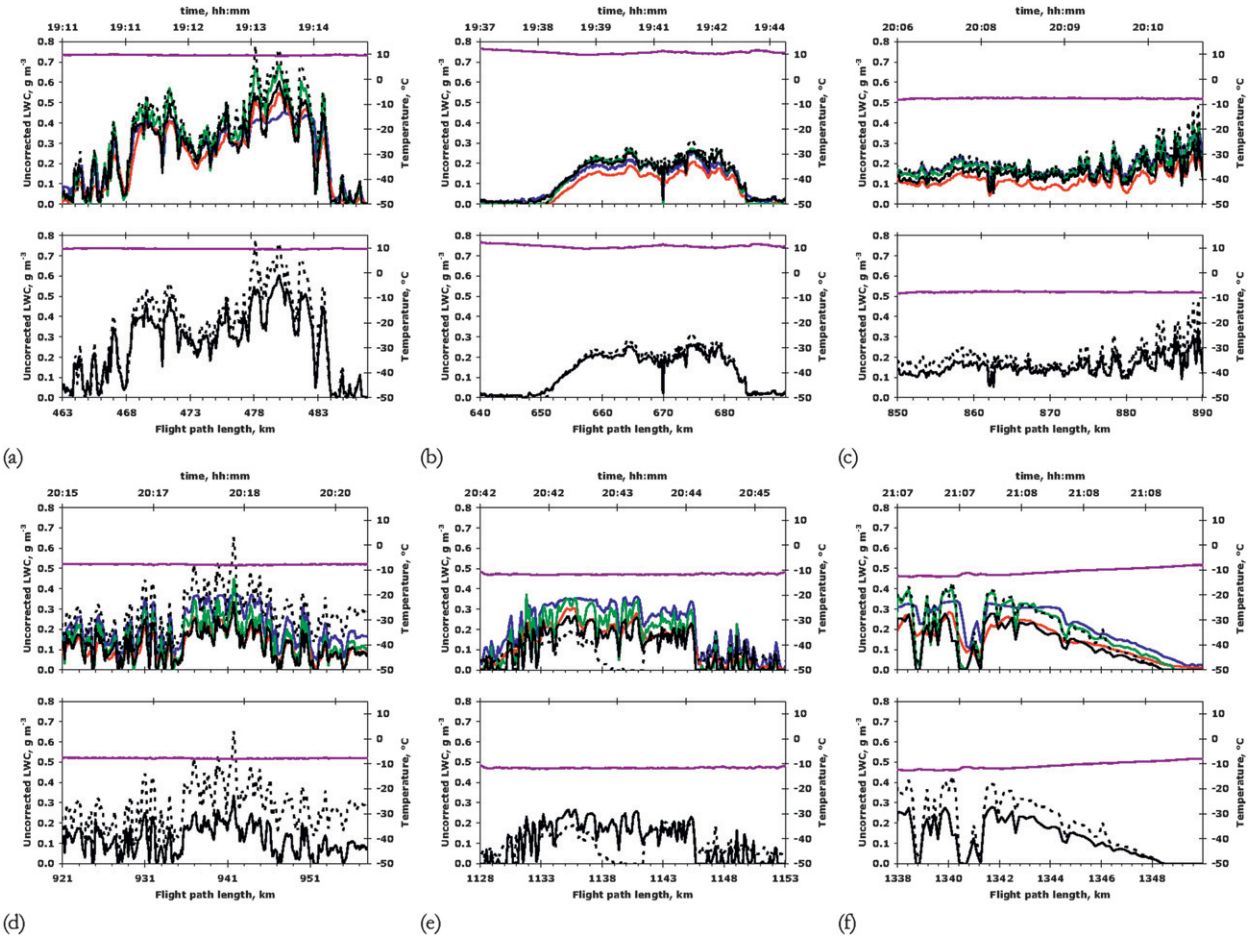

FIG. 9. LWC measurements from large T (blue), small T (red), Nevzorov (green), and two King (solid and dashed black) aircraft-mounted probes during AIRS II 109rf01 flight on 5 Nov 2003. Probe collection efficiencies, based on sensor size and shape and particle shape, size, and density, account for part of the differences between measurements.

concentration, while the small T probe reported a particle number concentration that was 20% lower. Figure 9d shows similar results, but the agreement between the two King probes was not as good as that in Fig. 9c, which in part can also be explained by a baseline offset. Figures 9e,f show different combinations of the agreement between the probes: Nevzorov and large T probes agreed well and reported the highest LWC; small T and King probe 1 (LWC1_Kin) matched, with a particle concentration that was 20%–30% below the previous two probes. In this case, the King probe 1, which in Figs. 9a,b reported the highest LWC, is now reporting the lowest LWC, perhaps resulting from ice accretion. Baseline drift is occasionally observed when the sensor builds up ice if the existing heaters are overcome by cold temperatures. The plots suggest that agreement between probes is better at warm temperatures than at low temperatures, perhaps because of ice accretion at low temperature.

2) ICE WATER CONTENT MEASUREMENTS

Measuring the water content of ice particles is a more complex problem than measuring LWC because additional variables, such as ice habit, particle density, and impaction efficiency, must be considered. Rogers et al. (2006) suggested that measurement differences arise from the range of particle sizes, the effect of probe location on the aircraft (fuselage, under wing, wingtip, pod), the time response, and the subcloud scale structure. Different probes present different collection efficiencies and capabilities to discriminate between small and large particles and high- and low-density particles because of their different geometry. Figure 10 shows measurements of IWC from the NCAR C-130 during the AIRS II 109rf12 flight on 1 December 2003, where small and large T probe measurements were plotted along with Nevzorov probe measurements. Different levels of agreement and disagreement between the

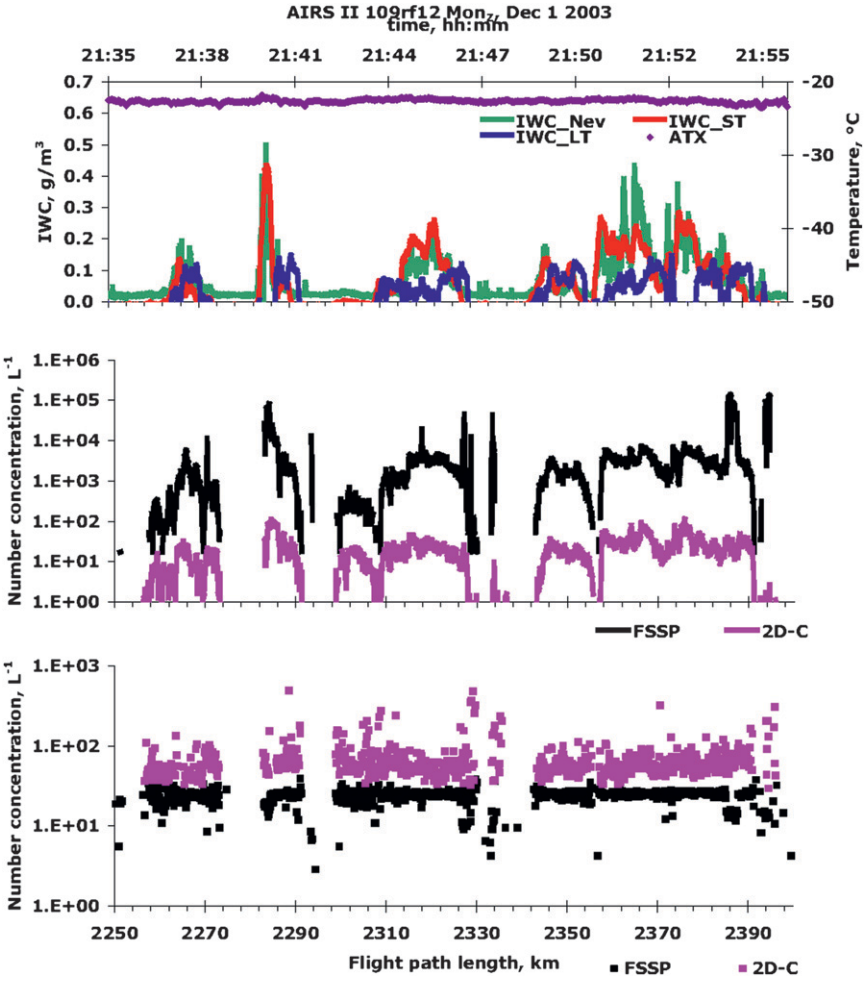

FIG. 10. IWC measurements from Nevzorov (green), small (red), and large (blue) T probes during flight AIRS II 109rf12 of 1 Dec 2003. Small T probe was mounted on the right wingtip, large T and Nevzorov probes were mounted about 1 m apart on the fuselage, and 0.5 m above the aircraft skin, inside the region where particle sorting occurs (<0.61 m; see Twohy and Rogers 1993).

probes are evident; often they responded at different times and/or indicated different magnitudes, suggesting different cloud properties. In general, the disagreement between large and small T probes and Nevzorov probes was larger when measuring IWC than when measuring LWC. For the same time interval, particles of 20-μm diameter were measured by the FSSP in concentrations ranging from 10^2 to 10^5 L^{-1}; meanwhile, larger particles (80 μm) were measured by the 2D-C probe in concentrations 2–3 orders of magnitude smaller. Correlation between small and large particles suggests particle breakup occurring at the inlet of the FSSP (Field et al. 2003; Korolev and Isaac 2005; Vidaurre and Hallett 2009b). Individual measurements of particle density following the approach presented in section 3a(2) ranged from 10 to 794 kg m^{-3}. Some of those crystals presented two or three layers of different densities. Hallett and Garner (2010) provide more details regarding ice crystals with densities that are dependent upon the radius. Depending on the principle of operation of the probes, IWC measurements may be influenced by the variation of the density along the radius of the particle. The use of empirical relationships relating the density of the particle with its size does not consider density variations along the radius leading to erroneous estimations. In addition, differences between probe measurements can in part be explained by local aerodynamic effects at sampling points around the aircraft (Twohy and Rogers 1993), and by actual differences in structure at subcloud size scales.

5. Conclusions

During numerous supercooled liquid cloud penetrations, two identical hot-wire LWC King probes tracked

generally well. The average difference between the two probes was below the instrument uncertainty (0.02 g m^{-3}). However, discrepancies of up to 0.1 g m^{-3} for 1-s LWC measurements of 0.3 g m^{-3} were observed. Disagreement between probes of different geometry and/or size was large, especially when detecting IWC. Differences in IWC measurements were attributed to different collection efficiencies of the instruments resulting from preferred particle size, shape, density, and local aerodynamic effects.

Each measurement is unique by nature of the conditions at only one point in time. With the available information from the AIRS II project it is difficult to generalize under what conditions the agreement between probes of different sizes and shapes is good; every case should be studied on a case-by-case basis. Analysis of data gathered with probes located at different places around the aircraft fuselage might provide useful insights about the microphysical structure of the cloud only if local aerodynamic effects and particle collection efficiency of each probe are considered.

The measurement of LWC by constant-temperature probes depends on the shape of the collector sensor, particle size distribution and density, airspeed and air density, location, and orientation of the sensor. Cloud microstructure defines the collection efficiency and thus affects LWC measurements. Because of these reasons, we do not expect probes of different geometries and sizes (or even identical probes) to provide the exact same measurements. Even the same droplet size distribution measured by the same probe at different altitudes and airspeeds may result in apparent different LWC.

The comparison of identical instruments on an aircraft either nearby or at different locations serves little purpose other than to offer a reality check in its broadest meaning to confirm their functionality. They necessarily must be responding to environments that are (or could be) different; it makes no sense to interpret differences in terms of location effects on the aircraft because separating these two effects is not a practical undertaking. A conclusion follows that the analysis of data from a single instrument, being aware of its limitations and capabilities, and subject to uncertainty beyond its threshold level, needs to satisfy an internal self-consistency criterion.

6. Recommendations

An adequate probe performance evaluation and intercomparison under controlled ice and liquid contents is necessary. This involves combining two identical airstreams with selected water drop spectra at selected temperature and air pressure with the capability of selectively nucleating one airstream and growing ice particles of a specific habit, size, and density. The system could be either horizontal or vertical, and the extent of mixing is controlled through choice of distance laterally and downstream. This study is also required to characterize the effect of particle bounce and breakup and the residual effect of ice particles on LWC measurement resulting from ice deposition at the forward stagnation line of the sensor.

Acknowledgments. This work was partially supported by a grant from National Science Foundation, Physical and Dynamic Meteorology Program ATM-0313581 as part of the AIRS II project, November 2003, and the *CloudSat* Program KM175-06-0063.

REFERENCES

Bailey, M. P., and J. Hallett, 2009: A comprehensive habit diagram for atmospheric ice crystals: Confirmation from the laboratory, AIRS II, and other field studies. *J. Atmos. Sci.,* **66,** 2888–2899.

Davison, A. C., and D. V. Hinkley, 1997: *Bootstrap Methods and Their Application.* Cambridge University Press, 582 pp.

Emery, E. F., D. R. Miller, S. R. Plaskon, W. Strapp, and L. Lillie, 2004: Ice particle impact on cloud water content instrumentation. *Proc. 42nd Aerospace Sciences Meeting and Exhibit,* Reno, NV, AIAA, Paper AIAA-2004-0731.

Field, P. R., R. Wood, and P. R. A. Brown, 2003: Ice particle interarrival times measured with a fast FSSP. *J. Atmos. Oceanic Technol.,* **20,** 249–261.

Gardiner, B. A., and J. Hallett, 1985: Degradation of in-cloud forward scattering spectrometer probe measurements in the presence of ice particles. *J. Atmos. Oceanic Technol.,* **2,** 171–180.

Hallett, J., 1980: Characteristics of atmospheric ice particles: A survey of techniques. Air Force Geophysics Laboratory, Air Force Systems Command, U.S. Air Force Rep. AFGL-TR-80-0308, 54 pp.

——, and L. Christensen, 1984: Splash and penetration of drops in water. *J. Rech. Atmos.,* **18,** 226–262.

——, and B. W. Garner, 2010: Measurement of growth and density of dendrite crystals. Preprints, *13th Conf. on Cloud Physics,* Portland, OR, Amer. Meteor. Soc., 8.2. [Available online at http://ams.confex.com/ams/pdfpapers/170124.pdf.]

——, W. P. Arnott, R. Purcell, and C. Schmitt, 1998: A technique for characterizing aerosol and cloud particles by real time processing. *PM2.5: A Fine Particle Standard. Proceedings for an International Specialty Conference,* J. Chow and P. Koutrakis, Eds., U.S. EPA and Air and Waste Management Association, 3198–3325.

——, R. Purcell, M. Roberts, G. Vidaurre, and D. Wermers, 2005: Measurement for characterization of mixed phase clouds. *Proc. 43rd AIAA Aerospace Sciences Meeting and Exhibit,* Reno, NV, AIAA, Paper 862.

Heymsfield, A., A. Bansemer, C. Schmidt, C. Twohy, and M. Poellot, 2004: Effective ice particle densities derived from aircraft data. *J. Atmos. Sci.,* **61,** 982–1003.

Hudson, J. G., 2007: Variability of the relationship between particle size and cloud-nucleating ability. *Geophys. Res. Lett.,* **34,** L08801, doi:10.1029/2006GL028850.

Isaac, G. A., A. Korolev, J. W. Strapp, S. G. Cober, F. S. Boudala, D. Marcotte, and V. L. Reich, 2006: Assessing the collection efficiency of natural cloud particles impacting the Nevzorov total water content probe. *Proc. 44th AIAA Aerospace Sciences Meeting and Exhibit,* Reno, NV, AIAA, Paper AIAA 2006-265.

King, W. D., and D. E. Turvey, 1986: A thermal device for aircraft measurement of the solid water content of clouds. *J. Atmos. Oceanic Technol.,* **3,** 356–362.

——, D. A. Parkin, and R. J. Handsworth, 1978: A hot-wire liquid water device having fully calculate response characteristics. *J. Appl. Meteor.,* **17,** 1809–1813.

Korolev, A. V., and J. W. Strapp, 2002: Accuracy of measurements of cloud ice water content by the Nevzorov probe. *Proc. 40th Aerospace Sciences Meeting and Exhibit,* Reno, NV, AIAA, Paper AIAA-2002-0679.

——, and G. A. Isaac, 2005: Shattering during sampling by OAPs and HVPS. Part I: Snow particles. *J. Atmos. Oceanic Technol.,* **22,** 528–542.

——, J. W. Strapp, and G. A. Isaac, 1998: The Nevzorov airborne hot-wire LWC-TWC probe: Principle of operation and performance characteristics. *J. Atmos. Oceanic Technol.,* **15,** 1495–1510.

——, E. F. Emery, J. W. Strapp, S. G. Cober, G. A. Isaac, M. Wasey, and D. Marcotte, 2011: Small ice particles in tropospheric clouds: Fact or artifact? Airborne Icing Instrumentation Evaluation Experiment. *Bull. Amer. Meteor. Soc.,* in press.

Langmuir, I., and K. Blodgett, 1946: Mathematical investigation of water droplet trajectories. *Collected Works of Irving Langmuir,* Vol. 10, Pergamon Press, 348–393.

Lasher-Trapp, S., S. Anderson-Bereznicki, A. Shackelford, C. H. Twohy, and J. G. Hudson, 2008: An investigation of the influence of droplet number concentration and giant aerosol particles upon supercooled large drop formation in wintertime stratiform clouds. *J. Appl. Meteor. Climatol.,* **47,** 2659–2678.

Noone, K. J., J. A. Ogren, J. Heintzenberg, R. J. Charlson, and D. S. Covert, 1988: Design and calibration of a counterflow virtual impactor for sampling of atmospheric fog and cloud droplets. *Aerosp. Sci. Technol.,* **8,** 235–244.

Ranz, W. E., and J. B. Wong, 1952: Impaction of dust and smoke particles on surface and body collectors. *J. Ind. Eng. Chem.,* **44,** 1371–1381.

Rogers, D. C., J. Hallett, A. Schanot, C. Twohy, J. Jensen, J. Stith, and G. Vidaurre, 2006: Comparison of LWC measurements on the NCAR C-130 in AIRS-2. Preprints, *12th Conf. on Cloud Physics,* Madison, WI, Amer. Meteor. Soc., P1.39. [Available online at http://ams.confex.com/ams/pdfpapers/113703.pdf.]

Schwarzenbock, A., and J. Heintzenberg, 2000: Cut size minimization and cloud element break-up in a ground-based CVI. *J. Aerosol Sci.,* **31,** 477–489.

Twohy, C. H., and D. Rogers, 1993: Airflow and water-drop trajectories at instrument sampling points around the Beechcraft King Air and Lockheed Electra. *J. Atmos. Oceanic Technol.,* **10,** 566–578.

——, A. J. Schanot, and W. A. Cooper, 1997: Measurement of condensed water content in liquid and ice clouds using an airborne counterflow virtual impactor. *J. Atmos. Oceanic Technol.,* **14,** 197–202.

——, J. W. Strapp, and M. Wendisch, 2003: Performance of a counterflow virtual impactor in the NASA icing research tunnel. *J. Atmos. Oceanic Technol.,* **20,** 781–790.

Vidaurre, G., and J. Hallett, 2009a: Ice and water content of stratiform mixed-phase cloud. *Quart. J. Roy. Meteor. Soc.,* **135,** 1292–1306.

——, and ——, 2009b: Energetics of mixed phase cloud particle interactions. *J. Atmos. Oceanic Technol.,* **26,** 972–983.